Intercluster interactions in rapid granular shear flows

M-L. Tan
Fluid Dynamics Research Center, James Forrestal Campus, Princeton University, Princeton, New Jersey 08544

I. Goldhirsch
Department of Fluid Mechanics and Heat Transfer, Faculty of Engineering, Tel-Aviv University, Ramat Aviv, Tel-Aviv 69978, Israel

(Received 21 August 1995; accepted 31 October 1996)

One of the possible phases of a sheared system of inelastically colliding rigid smooth disks is one in which relatively dense strips aligned at 45° to the streamwise direction are interspersed among similarly aligned dilute strips. The dense strips may have secondary microstructures in the form of elongated clusters. The latter are formed by an instability, following which they are convected, stretched, and rotated by the shear field. This process causes cluster–cluster collisions, a result of which is the partial destruction of the colliding clusters, followed by the emergence of new clusters. In addition, it is demonstrated that clustering dynamics can be responsible for hysteresis and multistability in granular systems. The studies presented in this paper involve molecular dynamics simulations complemented by theoretical analysis. © *1997 American Institute of Physics.* [S1070-6631(97)00203-1]

I. INTRODUCTION

A variety of rheological properties of granular systems in various flow regimes ranging from the quasistatic to the rapid regimes has been discovered in recent years. Many of them are reviewed e.g., in Refs. 1 and 2. Among these properties we wish to mention normal stress differences,[3,4] $1/f$ noise, nonlinear waves, convection rolls,[1] inelastic collapse,[5–7] sensitivity to boundary conditions, segregation,[8] layering, heaping,[9] and the formation of extended plugs.[10] Studies of the above phenomena, as well as of other effects that are found in granular systems, reveal that microstructures play an important dynamical role in such systems. The instability of granular systems to the creation of dense clusters or strips of various densities or compositions (in polydisperse systems) is by now well established. 'Pure' granular systems, i.e., collections of particles whose interactions are of dissipative nature, the effects of the ambient fluid being negligible, comprise just a small subset of the systems in which macroscopic particles are involved. In other particulate systems of interest, one observes significant microstructures as well. Examples include bidisperse particles sedimenting in a viscous fluid,[11,12] low-Reynolds-number sheared suspensions,[13] fluidized beds,[14] and more. The clustering processes in these suspensions bear an interesting, and perhaps far from superficial, similarity to those in granular flows; and the insights gained from the study of the latter flows (which are more accessible to numerical simulation) may be useful for the study of the former. In a sedimenting bidisperse suspension, for example, particles of the same species tend to coalesce in low-shear and high-velocity vertical streams that are surrounded by highly sheared "lubrication" layers of interstitial fluid.[11] These streams of particles separate into smaller streams as the relative velocity between the stream and the lubrication layer increases. This is reminiscent of the clustering process in granular flows, cf. Refs. 15 and 16. One of the results of the studies of clustering is the the identification of a length scale given by

$$L_* \approx \frac{l}{\sqrt{1-\bar{e}^2}}, \tag{1}$$

where l is the mean free path for the corresponding homogeneous flow and $\bar{e}$ is the coefficient of normal restitution. This length scale has been shown to represent the typical intercluster distance.[15,16] Thus, when the linear size of a system is smaller than L_* it cannot accommodate clusters but it can still be inhomogeneous; when it is larger than L_*, clustering will occur. The relevance of the above clustering mechanism to sheared systems (the work cited in Ref. 16 above refers to unforced systems) is one of the issues taken up in this work.

The rest of this paper is organized as follows: Section II provides a brief description of the systems we have studied and a detailed account of the cluster–cluster interaction mechanism. In Sec. III the Fourier spectra of the macrofields are examined and the scales and angles characterizing the systems under study are identified. In Sec. IV we present a study of the stability (both linear and nonlinear) of granular shear flows; in addition we demonstrate the existence of multiple steady states for a flow with a given set of external parameters and we relate this phenomenon to the clustering mechanism. Section V offers a brief summary of the findings of this work.

II. MICROSTRUCTURAL FEATURES

A. The model

The system considered here[17] consists of N identical smooth rigid disks of unit mass and diameter σ in a rectangular enclosure of size $L_x \times L_y$. This enclosure is periodically extended in both the x and y directions. Lees–Edwards boundary conditions,[18] i.e., periodic boundary conditions in the local Lagrangian frame (corresponding to the mean velocity profile) for shear flow are implemented. These boundary conditions correspond to the system being sheared by its

 1070-6631/97/9(3)/1/14/$10.00

periodic images that are adjacent to its top and bottom boundaries. These conditions were originally employed to study transport properties of simple fluids, and have also been used in simulations of granular systems.[4,19–21] They lead to a state of simple shear without having to formulate a wall boundary condition. An algorithmic definition of these boundary conditions, useful for implementation on the computer, can be found in Refs. 4, 17, and 21.

The only allowed interactions in the system are collisions of pairs of disks. The collisions occur either between two disks lying within the enclosure or between a disk in the enclosure and another disk in a periodic image of the enclosure. The velocity of each disk is constant between collisions. The collision process is characterized by a constant coefficient of normal restitution, $\bar{e}$, with $0<\bar{e}\leq 1$, which, when combined with the conservation of linear momentum, determines the outcome of the collision.

The initial condition of the simulation is similar to that used in Refs. 17 and 21 and it corresponds to the sheared configuration of an elastic hard-disk gas with a mean linear velocity profile. As shown below, the mean velocity profile persists throughout the simulation in spite of the fact that the system becomes highly inhomogeneous—this is a consequence of using the Lees–Edwards boundary condition. The numerical method used for the simulation is the "event-driven" method[22] (modified to incorporate the Lees–Edwards boundary condition—cf. Ref. 17 and references therein).

B. Microstructures

The parameters characterizing the system are: $\bar{e}$, N, L_x, and L_y mentioned above, $\bar{\nu}$, the mean area (volume) fraction of the particles and $\pm U/2$, the (effective) velocities of the upper and lower boundaries of the enclosure, respectively. In most of the paper we consider two specific sheared systems, which we refer to as System I and System II. The parameters of System I are given by: $\bar{e}=0.9$, $N=20000$, $U=100$, $L_x=L_y=1$, and $\bar{\nu}=0.05$; the parameters of System II are given by: $\bar{e}=0.6$, $N=200000$, $U=100$, $L_x=L_y=1$, and $\bar{\nu}=0.05$. These parameters determine the particle diameter σ and mean free path l, which are given, for System I, by $\sigma=0.001\,78$ and $l\approx 1/71$, and for System II, by $\sigma=0.000\,564$ and $l\approx 1/226$ (the mean free path in a two-dimensional system of disks is $l=L_xL_y/2N\sigma$). Both systems are dilute but System I is nearly elastic while System II is highly inelastic. The reason the number of particles in System I is much smaller than that in System II is that we wish to demonstrate that the bifurcation between quasihomogeneous and highly inhomogeneous states depends on the ratio of the typical intercluster distance, L_*, given by Eq. (1), to the linear size of the system. The parameters for System I are chosen so that the value of L_* for this system is much larger than that corresponding to System II. The properties of a quasihomogeneous system (which is also a "small" system since the condition of the system size being smaller than L_* is equivalent, in the case of a fixed system (area) volume, to the number of particles in the system being smaller than a given threshold) are qualitatively different from those of an inhomogeneous (or "large") system. In particular, clusters

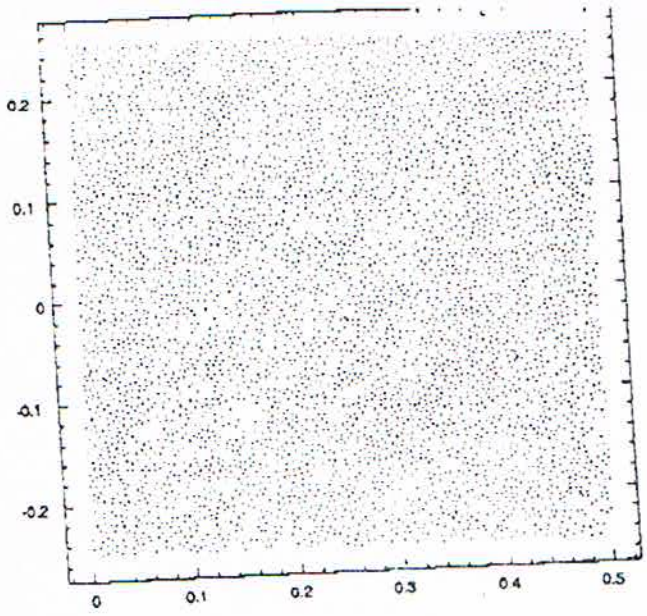

FIG. 1. The particle configuration for System I. The portion of the flow domain shown here corresponds to a square region in the center of System I whose area is 1/4 the area of System I. The time here corresponds to 200 collisions per particle following the initial condition.

are created only in large systems but not in small systems and the values of the average stresses in small systems are closer to the predictions of kinetic theories of granular flows than those in large systems.

A plot of the particle configuration of (part of) System I at a time corresponding to the lapse of 200 collisions per particle following the initial condition is shown in Fig. 1. The full flow domain is not shown in Fig. 1 because scatter plots systems consisting of 20 000 or more particles tend to be inadequately resolved when reproduced in the journal. The portion of the flow domain shown in Fig. 1 corresponds to a square region in the center of System I whose area is 1/4 the area of System I. The values of the average granular temperature and other statistical characterizations of the system are stationary at this time. The density contour plot (of the whole system), Fig. 2, shows that weak flow-scale inhomogeneities in the form of thick strips aligned along the extensional axis of the shear and spanning the system exist in the flow. The arrangement of these strips is such that the denser strips are interspersed among less dense strips of a similar size and orientation. The internal structure of these strips, though still weakly inhomogeneous, does not contain the discernible dense clusters that exist in highly inelastic sheared systems. The spatial structure of the kinetic and collisional pressure fields (not depicted here) is similar to that of the density field, that is, it consists of diagonal and weakly inhomogeneous strips that span the linear dimension of the flow.

A plot of the particle configuration of System II at a time corresponding to the lapse of 100 collisions per particle following the initial condition is shown in Fig. 3. The portion of the flow domain shown in Fig. 3 corresponds to a square

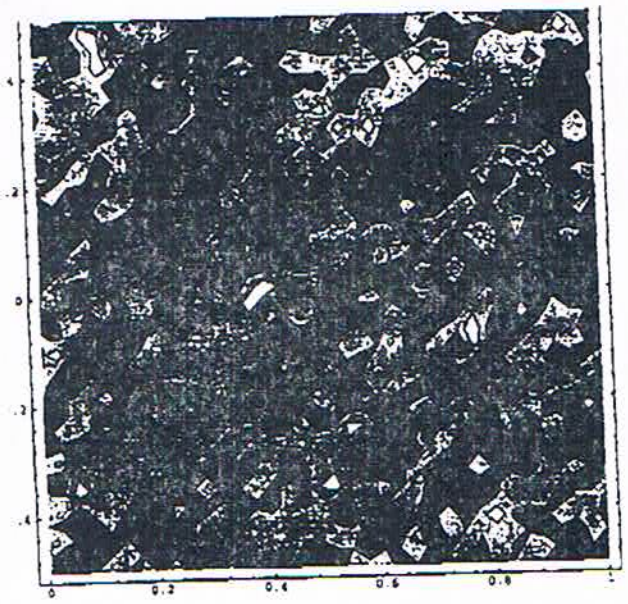

FIG. 2. The density field for System I at a time corresponding to 200 collisions per particle following the initial condition. The shade code is: lighter gray for higher densities and darker for lower densities with the lightest shade corresponding to a value equal to 80% of the full range of densities observed in the flow and the darkest shade to 20% of this range. The intermediate shades are equally spaced. The density ranges from 70% to 130% of its average value.

region in the center of System II whose area is 1/16 the area of System II. It is evident that dense and anisotropic local agglomerations of particles occur throughout the flow field in the form of elongated clusters. Most clusters are oriented at approximately 45° with respect to the streamwise direction (i.e., in the extensional direction of the flow) and some clusters are oriented at smaller angles with respect to the streamwise direction. A stripwise organization of the clusters in System II can still be discerned, though the strips in this case are "pinched" and "bent" in several places along their lengths and do rarely span the system, in contrast to those found in System I. Just as the dense strips in System I are interspersed among dilute strips of a similar orientation and size, the clusters in System II are also interspersed among relatively dilute regions of a similar shape, orientation, and size. The temperature is lower in the interior of the clusters than in the ambient dilute region. Developing clusters are also characterized by lower pressure, though in "mature" clusters (which do not grow any further), the pressure is approximately equal to that in the ambient. While the clusters are relatively dense, the typical area fraction inside a cluster (in our simulations) is about twice the average area fraction (0.05 in our simulations). Thus the clusters, in the case considered here, are relatively dilute as well. This is a result of the continual energy replenishment (and consequently thermalization) by viscous heating due to the shear field. Still, in denser systems (not described here) some clusters may reach maximal packing, probably by the collapse effect.[6]

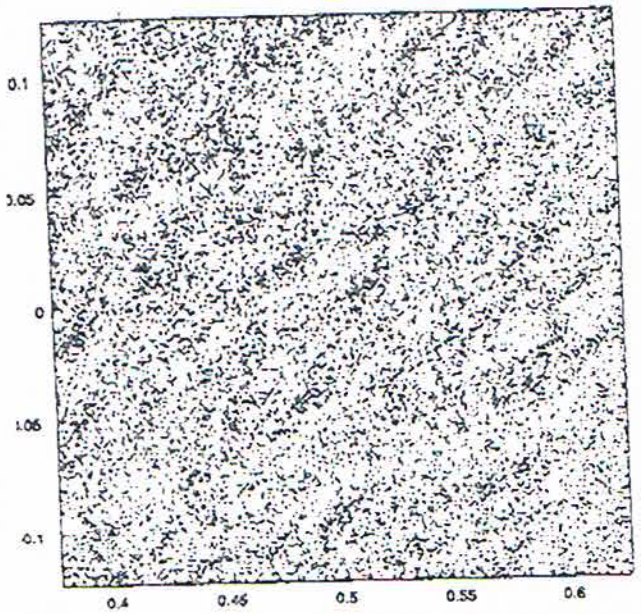

FIG. 3. The particle configuration for System II. The portion of the flow domain shown here corresponds to a square region in the center of System II whose area is 1/16 the area of System II. The time here corresponds to 100 collisions per particle following the initial condition.

C. Cluster–cluster interaction

The stripwise microstructure described in Sec. II B has been observed in previous computer simulations;[21] the orientation of the strips has been theorized upon in Refs. 23–25. These studies, which are based on equations derived in Refs. 26 and 27, have discovered (through linear stability analysis) modes that grow transiently but decay at asymptotically long times. They have found that the leading instability corresponds to a wave vector whose direction is at 45° with respect to the streamwise direction. Such a wave vector corresponds to structures which lie at 135° to the streamwise direction in contrast with numerical findings. The resolution of this problem is presented in Sec. IV.

As mentioned above, System II possesses a clustering instability which occurs within the oblique dense layers. The emerging clusters are then distorted, convected and rotated by the flow. Since they are identifiable on relatively long time scales (with respect to the inverse shear rate) and one can actually follow the motion of single clusters in a "movie" depicting their dynamics, they can be considered to be coherent (micro)structures. Since the temperature inside the clusters is relatively low, the particles in the clusters follow (practically horizontal) trajectories that are roughly dictated by the mean flow; as a result the clusters *appear* to rotate and be stretched as if they were deformable solid bodies. Moreover, they scatter into each other as they are being convected, thus producing a very complex dynamics that involves rapid dispersion and reorganization of mass in the flow. Nevertheless, the stripwise clustering microstructure persists. We propose that it is by means of the cluster–cluster interactions, hand-in-hand with the nonlinear clustering process, that this type of oblique microstructure is maintained in the flow.

Our numerical results reveal that the velocity fields in both System I and System II correspond to an extremely uniform linear shear field at all times. This is the case despite

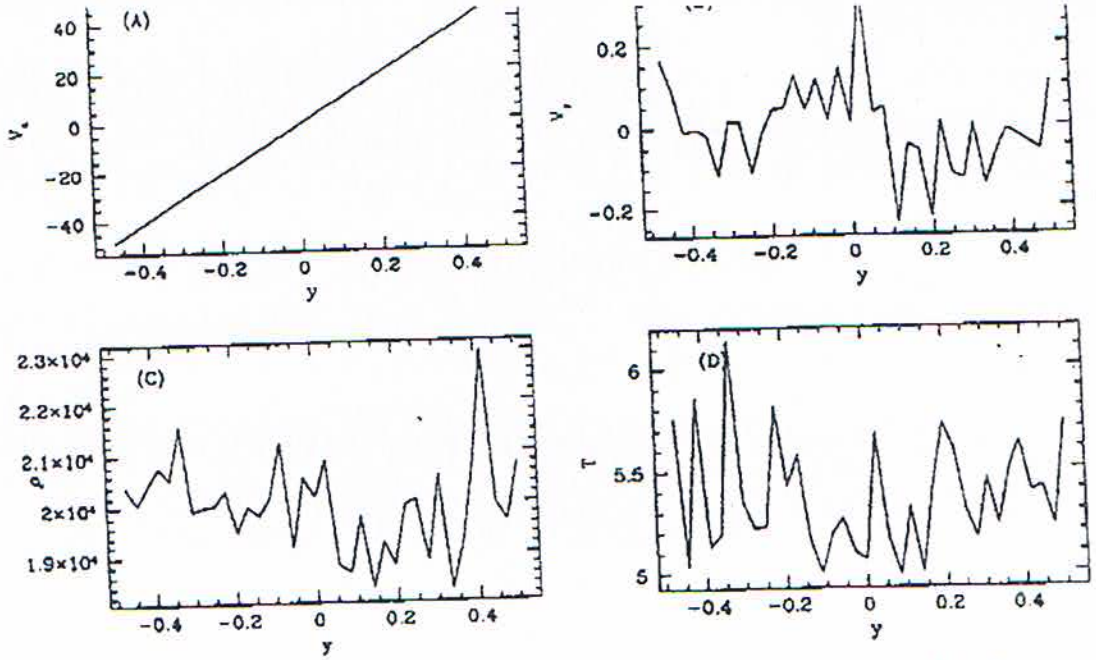

FIG. 4. Streamwise-averaged flow properties for System I: (A) the velocity component V_x; (B) the velocity component V_y; (C) density ρ; (D) temperature T. Notice that all profiles are essentially uniform, the relative fluctuations being very small.

the rapid temporal variations in the spatial structures of both systems. Some other streamwise-averaged properties for System I and System II, such as their temperature and number density profiles, are presented in Figs. 4 and 5. These profiles show variations with typifiable length scales on an essentially flat background.

It is convenient to express the two-dimensional uniform shear field, $\mathbf{V}(x,y)$, with shear rate γ as $\mathbf{V}(x,y)=(\gamma/2)[(y,x)+(y,-x)]$. The velocity field corresponding to the first term in the square brackets is an irrotational stretching field which tends to compress a flow structure along the 135° direction and stretch it along the 45° direction. The velocity field corresponding to the second term in the square brackets represents a clockwise rotation of the system. Thus, as mentioned, all structures in the shear flow are permanently and simultaneously compressed, stretched and rotated by the flow. One may then presume that at any instant of time there should be clusters aligned at all possible angles of inclination. Indeed the clusters start off at approximately 45° and are rotated in the clockwise direction. Since the longer the cluster is rotated, the more likely it is to collide with adjacent clusters and be dispersed by the collision, a distribution of angles of inclination for the clusters indeed emerges. However, this distribution is strongly weighted towards angles close to 45° and it tails off as the angle becomes smaller. The power spectrum of the density, presented in Sec. III corroborates this observation. An explanation of this fact is proposed below.

The practically fixed orientation of the clusters can be understood by closely following their dynamics. The kinematics of cluster interaction can be described with the help of a sequence of closely cropped contour plots that show the density field around two neighboring clusters at successive instants of time. Figure 6 depicts a sequence of contour plots of the density field in a small window that is just large enough to show a few clusters lying within two adjacent dense strips. These plots are produced from snapshots of System II at successive instants of time which are separated by time intervals that corresponds to the lapse, on the average, of 0.25 collisions per particle in the system (i.e., a total of $N/4$ collisions, where N is the number of particles in the system, have occurred between one plot and the next). Figure 6(A) shows two clusters that were oriented approximately along the extensional axis of the shear with the cluster labeled A in the figure lying above and to the left of the cluster labeled B. In Fig. 6(B), which shows the density field 0.25 collisions per particle later, both clusters A and B have rotated slightly away from the extensional axis and they are closer to each other. They have also been slightly stretched along the extensional axis by the flow. The fact that the clusters appear to be "drawn" closer to each other is *not* a dynamical effect, such as an effective interaction between the clusters; it is merely a kinematic effect that results entirely from convection. This conclusion follows from the fact that the motion of each cluster as a whole is found to closely match the motion dictated by the average velocity field (and, as mentioned, the temperature inside the clusters is relatively low).

Since the velocity field is linear, the velocity profile seen from a local frame of reference moving at the local value of the (mean) velocity is identical to the global profile. It can thus be decomposed in a similar way into a rotational part and a stretching/compressing part. Clusters viewed in the local frame appear to rotate about the origin of the frame, and two clusters that are close enough together and whose geometric centers lie approximately along the same horizon-

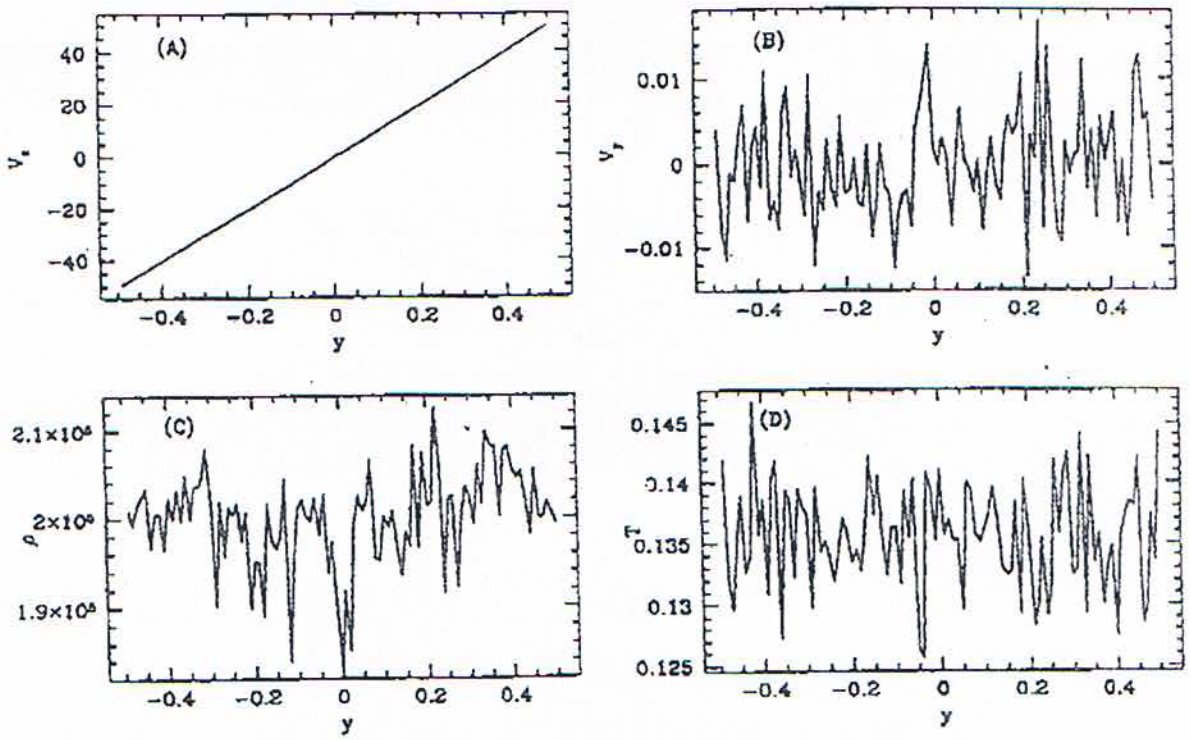

FIG. 5. Streamwise-averaged flow properties for System II: (A) V_x; (B) V_y; (C) density ρ; (D) temperature T. Notice that all profiles are essentially uniform, the relative fluctuations being very small.

tal line must collide with each other as they are being rotated. This is roughly the situation with the two clusters shown in Fig. 6. The collision that occurs between them is depicted in Figs. 6(C) and 6(D); in the former figure, the bottom half of cluster B is seen to have begun to scatter into cluster A, creating an expanded region of dispersed particles (though still of moderately high density). Then, in the latter figure, a "mass attractor" (i.e., a clustering center), labeled M, forms out of this region while the top half of cluster B breaks away from what is now the amalgamation of its lower half with cluster A. This amalgamation is then compressed in the 135° direction and stretched in 45° direction by the shear, causing a new cluster elongated along the latter direction to take shape. This cluster becomes more fully formed in Fig. 6(E) and is labeled C. It can be also be seen in Fig. 6(E) that the top half of cluster C is about to scatter into the bottom half of cluster B' [which is the broken-off descendant of cluster B in Fig. 6(C)]. The outcome of this scattering is again a dilated region of dispersed particles as shown in Fig. 6(F), and the cycle of formation of a new cluster through the appearance of a mass attractor in this region then repeats. The fact that the scattering produces a dilated region is evidently due to the fact that part of the kinetic energy of the colliding clusters is converted into thermal energy and, as a result, the temperature and pressure in the region are raised and cause a dispersion of the particles in that region.

The paradigm of this process of cluster convection and cluster scattering followed by dilation and mass reorganization applies throughout the system. Hence, even though the spatial orientations of the clusters in the system appear to remain mostly along the extensional axis, what actually happens is that new clusters are being continually created in this direction. The structure of the other field variables, such as the temperature, kinetic and collisional stress tensors, follow this time-dependent paradigm: A local organized inhomogeneity is first created along the extensional axis and is convected and then dispersed or modified by cluster interactions before a new inhomogeneity is reorganized in its place. Since a region of average density in the flow is always (nonlinearly) unstable with respect to the creation of clusters, the mass reorganization stage that follows the dilation stage is due to the same nonlinear clustering mechanism that is responsible for the creation of diagonally aligned clusters from the initial uniform density field. In summary, the stripwise clustering microstructure in simple granular shear flows is stabilized through the combined effect of a nonlinear clustering instability, cluster convection and a complex process of cluster interaction and mass reorganization.

III. SPECTRAL ANALYSIS

This section is devoted to the presentation of the Fourier spectra of the density and momentum fields of System I and System II as well as other sheared systems characterized by different external parameters. One of the results presented below is that the typical length scale in the density fields of systems with different values of the coefficient of restitution, $\tilde{e}$, is approximately given by relationship (1).

The Fourier transforms of the mass and momentum densities are:

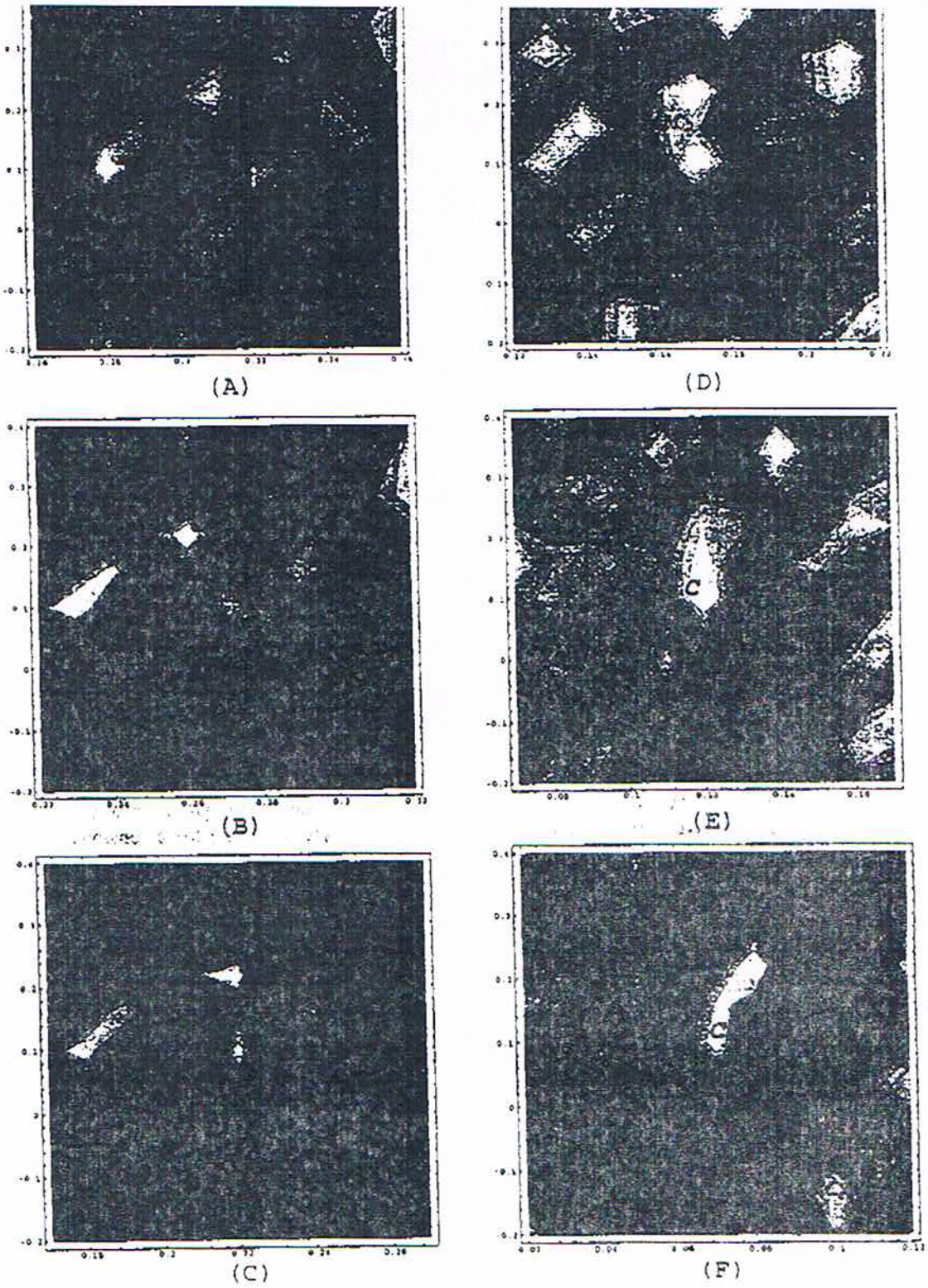

FIG. 6. A close view of the density field at successive instants of time around two clusters interacting with each other. The shade code for the contour plots is: lighter greys for higher density and darker for lower densities. A detailed explanation of the plots is provided in the text.

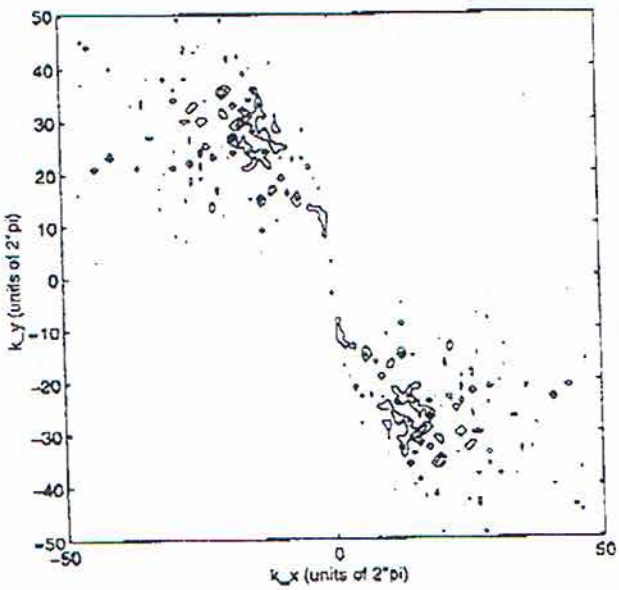

FIG. 7. Contour plot of the power spectrum of the density field of System II. The contour lines corresponds to equally spaced values of the spectrum from 20% to 80% of the full range observed.

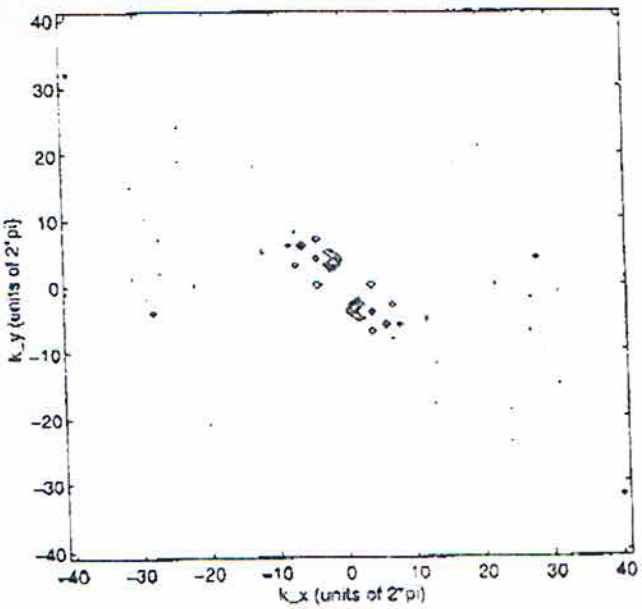

FIG. 8. Contour plot of the power spectrum of the density field of System I. The contour lines corresponds to equally spaced values of the spectrum from 20% to 80% of the full range observed.

$$\tilde{\rho}(\mathbf{k}) \equiv \frac{m}{2\pi} \sum_{j=1}^{N} \exp(i\mathbf{k}\cdot\mathbf{r}_j)$$

and

$$\tilde{\mathbf{p}}(\mathbf{k}) \equiv \frac{m}{2\pi} \sum_{j=1}^{N} v_j \exp(i\mathbf{k}\cdot\mathbf{r}_j),$$

respectively, where $\mathbf{r}_j$ is the position vector of particle j in the system. The allowed values of the wave vectors are determined by the boundary conditions. In our case the (Lees–Edwards) boundary conditions are periodic in the Lagrangian frame for shear flow—i.e., they are periodic only after a local Galilean transformation that depends on the local mean velocity has been applied to the coordinate system. The (time dependent) allowed wave vectors are obtained as follows. Let $\mathbf{a}_1$ and $\mathbf{a}_2$ be the "basis vectors" for the lattice consisting of the system and its periodic images. Let $\bar{p}$ be an integer such that $0<L_y\gamma t-\bar{p}L_x<L_x$, and define $[\gamma t]=\gamma t-\bar{p}L_x/L_y$. Then we have $0<[\gamma t]<L_x/L_y$ and the basis vectors can be written as $\mathbf{a}_1=(L_x,0)$ and $\mathbf{a}_2=([\gamma t]L_y,L_y)$. The basis vectors for the corresponding reciprocal lattice are:

$$\mathbf{k}_1=\left(\frac{2\pi}{L_x},-\frac{2\pi[\gamma t]}{L_x}\right) \quad \text{and} \quad \mathbf{k}_2=\left(0,\frac{2\pi}{L_y}\right).$$

The time dependence of this vectors does not change the (standard) interpretation of spectra, it just affects the distribution of the allowed (discrete) wave vector values at each instant.

Figure 7 shows a contour plot of the power spectrum of the density field for System II. The contours in Fig. 7 correspond to equally spaced values between the minimal and maximal values of the spectrum. It is evident that the dominant wave vectors are aligned at angles between 90° and 135° with respect to the positive k_x axis. This implies that spatial structures in the density field are aligned at angles between 0° and 45°, in agreement with the direction of the structures observed in Fig. 3. The corresponding spectrum for System I is shown in Fig. 8. The dominant wave vectors are again aligned between 90° and 135°, though their magnitudes are smaller than those of the dominant wave vectors in System II, indicating that the spatial scales in the density field in System I are larger. Since the mean free paths in the two systems are different, we cannot directly compare their spatial scales. However, the comparison can be made if these scales are expressed in units of the mean free paths of the corresponding systems; if this is done, we find that the scales in System I are still larger than those in System II.

The power spectrum, $\mathbf{P}(\mathbf{k})$, of the momentum field is presented separately for the x and the y components of the field. The part of the momentum field due to the linear shear profile does not affect the power spectrum except at points on the k_y axis. Let the macroscopic momentum field, $\mathbf{p}(\mathbf{r})$, be written as $\mathbf{p}(\mathbf{r})=\rho(\mathbf{r})\gamma y\hat{\mathbf{x}}+\mathbf{p}'(\mathbf{r})$, where $\hat{\mathbf{x}}$ is the unit vector along the x axis and $\mathbf{p}'$ denotes the deviation of the field from the value that corresponds to the linear velocity profile alone. It is easy to check that the spectrum of $\rho\gamma y\hat{\mathbf{x}}$ with constant density (ρ) is nonzero only for $k_x=0$ (i.e., on the k_y axis). Density variations affect this conclusion in a minor way (see below). If instead of computing the Fourier transform of $\mathbf{p}(\mathbf{r})$ we compute the Fourier transform of $\mathbf{p}'(\mathbf{r})$, i.e., of $\tilde{\mathbf{p}}'(\mathbf{k})=m\sum_{j=1}^{N}(\mathbf{v}_j-\gamma y_j\hat{\mathbf{x}})\exp(i\mathbf{k}\cdot\mathbf{r}_j)$ where y_j is the y coordinate of the jth particle in the system, we eliminate most of the power at the points on the k_y axis that is due to the average profile. However, this power is not completely eliminated, since a global trend (i.e., a variation whose length scale is of the order of the linear dimension of the

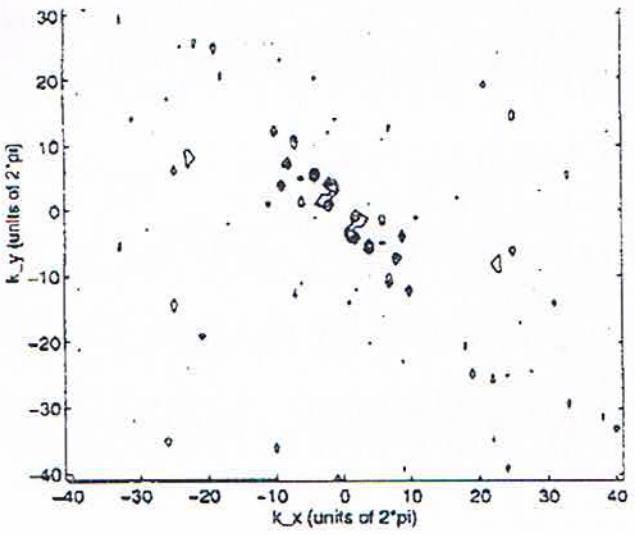

FIG. 9. The power spectrum P_x of the x component of the momentum field of System I. The contour lines corresponds to equally spaced values of the spectrum from 20% to 80% of the full range observed.

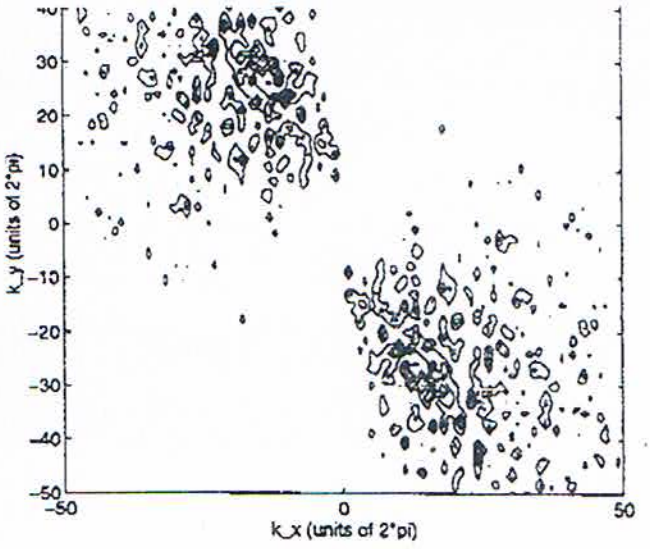

FIG. 10. The power spectrum P_x of the x component of the momentum field of System II. The contour lines corresponds to equally spaced values of the spectrum from 20% to 80% of the full range observed.

system) exists in $\mathbf{p}'$ due to the fact that the total momentum of the system fluctuates around zero (a consequence of the boundary conditions). This fluctuation appears to be thermal in nature and its magnitude is $O(N^{-1/2})$ times the magnitude of the total momentum in, say, the top half (i.e., $0<y<L_y$) of the system. As a result of this fluctuation, the magnitude of the total momentum in the top half of the system is different from that of the total momentum in the bottom half. However, the values of $\tilde{\mathbf{p}}'(\mathbf{k})$ at points on the k_y axis are still about one order of magnitude larger than the power of the more interesting off-axis structures in the spectrum. Hence we have chosen to ignore the power on the k_y axis in the $\tilde{p}'_x$ spectrum. Although a global trend may also exist in $\tilde{p}'_y$, its magnitude is very small compared to the trend in $\tilde{p}'_x$ (since the mean y component of the momentum is zero) and it does not pose a problem to the interpretation of the spectrum. Since we have ignored the power on the k_y axis in the $\tilde{p}'_x$ spectrum, we have also ignored possible horizontal layering structures in the velocity field. However, we have checked that the power at large values of k_y on the k_y axis (at which the power due to the global trend in $\tilde{p}'_x$ is negligible) is small, and thus there is no horizontal layering in the velocity field (as can be checked directly by studying the particle scatter plot).

A contour plot of the spectrum P_x of the momentum field for System I is shown in Fig. 9; the corresponding spectrum for System II are shown in Fig. 10. The P_y spectra for both systems have the same structure as the corresponding P_x spectra. These figures show that most of the peaks in P_x lie between 90° and 135° with respect to the positive k_x direction, with the stronger peaks lying at angles closer to 135°. Thus, the structure of the x component of the momentum field, much like the structure of the density field, consists of differentiated strips aligned mostly along the extensional axis of the shear. This structure can be understood as follows: Consider the x component of the mean velocity along a line parallel to the x axis which cuts the alternatingly dense and dilute strips. This velocity is in general not equal to the value that is obtained by interpolating between the values of the velocities at the top and bottom boundaries, but it does fluctuate around the interpolated value. The deviations from the interpolated value are smallest at points that correspond to the center of each dense or dilute strip and are correspondingly largest at the edges of each strip. This variation corresponds to the alternation of regions into which particles are converging, i.e., the denser strips, with regions from which particles are diverging, i.e., the more dilute strips, with the converging or diverging flows being strongest at the edges but "stagnant" at the center of each strip. A similar argument holds for the y component of the momentum field. The above results also hold for systems having aspect ratios different from unity, in particular the orientation of the strips is the same. Thus the structure described above is of dynamical origin and not due to geometry.

The typical intercluster separation L_*, cf. Eq. (1), which was originally predicted for (dilute) *free* granular systems, is valid for sheared systems as well. It exhibits an area fraction dependence, as shown below. Figure 11 presents the results of a series of simulations with different values of $\tilde{\epsilon}$ and two values of the homogeneous solid fraction, denoted by $\bar{\nu}$, equal to 0.05 and 0.10, the other parameters being held fixed. It is observed that for a given value of $\bar{\nu}$, which is equivalent to a given value of l, the dominant scale as determined from the spectral analysis varies linearly with L_* (the measured value of this scale is denoted by L_0). Figure 12 presents plots the data from two-dimensional simulations of simple shear flows obtained by Hopkins and Louge,[21] in which their data

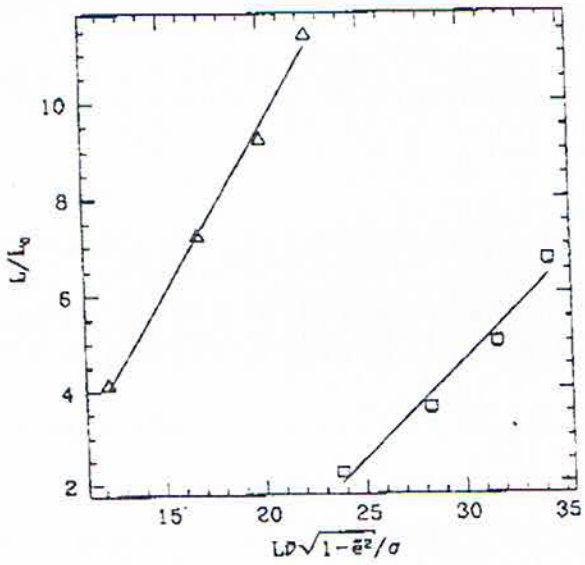

FIG. 11. The dominant length scale L_0/L (where L is the linear dimension of the system) in the density field as a function of $L\bar{\nu}\sqrt{1-\bar{e}^2}/\sigma$ at fixed $\bar{\nu}=0.05$ (corresponding to △) and $\nu=0.1$ (corresponding to □). The number of particles in the system is 20 000.

is rescaled in terms of L/λ and $L\bar{\nu}\sqrt{1-\bar{e}^2}/d$ as ordinate and abscissa respectively (where L is the linear dimension of the system), d is the particle diameter (notation used in Ref. 21) and λ is the dominant scale obtained by Fourier analyzing the density field (again notation used in Ref. 21). While somewhat more noisy (due to a smaller number of particles in their simulation), the Hopkins and Louge data confirms the above properties of the typical length scale. The slopes of the graphs of L/L_0 vs $L\bar{\nu}\sqrt{1-\bar{e}^2}/\sigma$ as a function of the

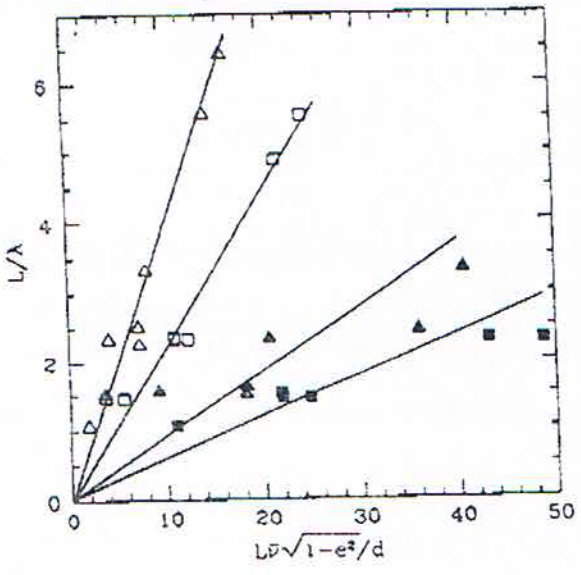

FIG. 12. Results of two-dimensional simple shear flow simulations presented originally in Ref. 21 but organized here using the scaling in Fig. 11. Here L is the linear dimension of the flow; d is the particle diameter and λ is the dominant length scale observed in the density field. The data points △, □, ▲, and ■ correspond, respectively, to $\bar{\nu}=0.1$, 0.3, 0.5, 0.6. The straight lines are drawn through the data points to guide the eye.

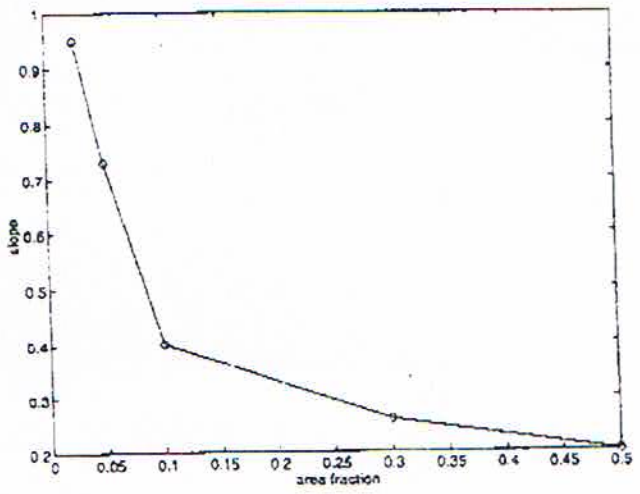

FIG. 13. The slopes measured off the functional dependence of L_0/L vs $L\bar{\nu}\sqrt{1-\bar{e}^2}/\sigma$ for a number of area fractions.

mean area fraction, $\bar{\nu}$, are presented in Fig. 13. It is clear from the latter figure that the slope approaches unity in the limit of low area fraction (the original theory is based on equations of motion derived from the Boltzmann equation and thus it is reliable in the low area fraction regime). As the area fraction increases the slopes become smaller, as the intercluster distance approaches the interparticle distance (as one would expect in the limit of close packing). Thus, while some of the quantitative details regarding the nature of clusters depend on density and on the specific system (here—a sheared system) the basic mechanism responsible for clustering in freely decaying flows, as expounded in Ref. 16, applies to shear flows (including dense flows) as well.

IV. STABILITY ANALYSIS AND TIME SCALES

The process of clustering is faster the higher the average granular temperature in the system. The degree of clustering or of the inhomogeneity of the system strongly depends on the rate of this process relative to those of competing processes such as diffusion and convection. Consequently, a sheared system in which the granular temperature is relatively high (e.g., one prepared in an initial state whose average granular temperature is much higher than that in the statistically steady state to which the system eventually evolves) exhibits a markedly different dynamics from one in which the (initial) temperature is low, all other externally imposed parameters for the two systems being the same. This is one of the sources of hysteretic behavior in granular systems, as further expounded below. It leads to the existence of multiple steady states which correspond to the same external parameters but which are characterized by very different microstructures.

The numerically observed time scale for cluster creation is very short in inhomogeneous systems (about a third of the inverse shear rate) but it takes about 10 inverse shear rate times for the initial condition to saturate to the asymptotic statistically steady state (cf. Fig. 14). It seems conceivable that a linear stability analysis in which the convective terms

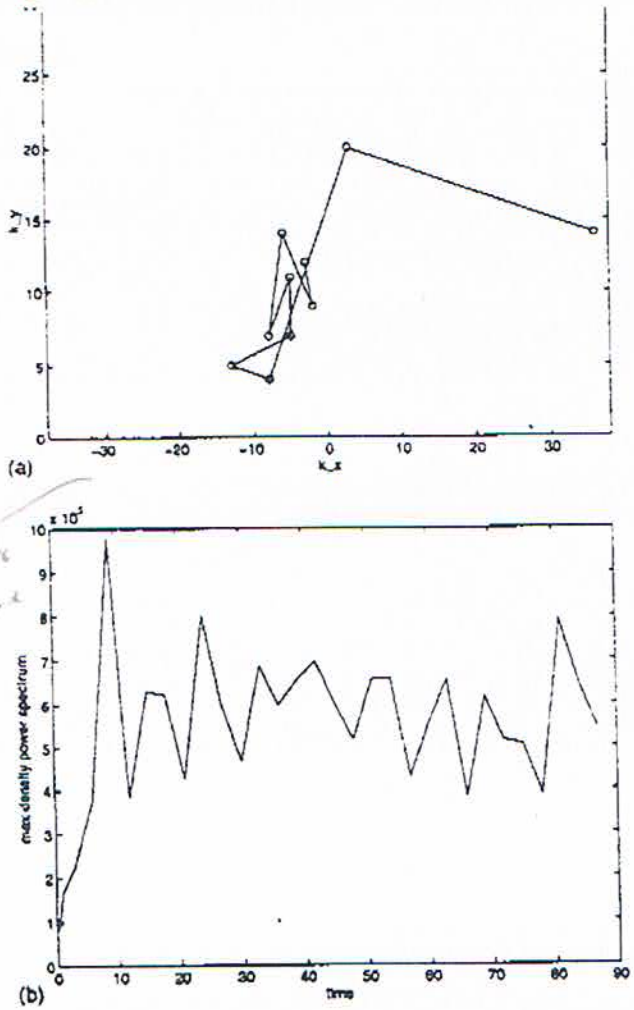

FIG. 14. (A) The time dependence of the wave vector corresponding to the strongest peak in the power spectrum of the density. The rightmost circle corresponds to a time following 0.2 collisions per particle after the initial time, consecutive times are separated by three collisions per particle. The parameters of this system are: $N=20\,000$, $\tilde{e}=0.6$, and $\bar{\nu}=0.05$. (B) The maximal value of the density power spectrum, in the same system as described in (A), as a function of time.

of the equations are neglected should signal the layering/clustering instability, which is observed to commence in a very short time. As shown in the next section, the results of such a stability analysis (which differs from those of Schmidt, Savage, and Babic, quoted below, since the convective terms are ignored) do indeed confirm the instability of the basic homogeneous state but they fail to account for the rate of growth of this instability. One may conclude that nonlinear effects take over at a very early stage of the dynamics that gives rise to layers and clusters.

A. Transient linear instability of shear flows

In previous work[23–25] a transient instability was found to exist in homogeneous (uniform density) states in which the velocity profile is linear. As mentioned above, these stability analyses find that the wave vector corresponding to the most unstable mode points at 135° (in real space) with respect to the streamwise direction, in contrast with numerical findings, tioned on the basis of the low growth rates predicted by it (see below), it is interesting to note that the next transiently most unstable mode corresponds to disturbances in real space that lie along the 45° direction. Numerical simulations [cf. Fig. 14(a)] show that the initial instability (with respect to the homogeneous state) indeed occurs mostly in the 135° direction, as expected on the basis of linear stability analysis, then the mode corresponding to the 45° direction is accented. Thus, while, as mentioned, linear stability analysis produces disturbingly low growth rates, it does capture some of the properties of the observed instabilities.

Consider the nearly elastic low density limit of the Jenkins–Richman equations (cf. Ref. 28):

$$\nu(\dot{T}+v_i\partial_i T)=\frac{\sqrt{\pi}}{2}\sigma\partial_i(\sqrt{T}\partial_i T)-\nu T\partial_i v_i + \frac{\sqrt{\pi}}{4}\sigma\sqrt{T}\,\mathrm{Tr}\,\hat{D}_{ij}^2-\frac{4}{\sqrt{\pi}}\frac{\nu^2}{\sigma}\epsilon T^{3/2}, \quad (2)$$

$$\nu(\dot{v}_j+v_i\partial_i v_j)=-\partial_j(\nu T)+\frac{\sqrt{\pi}}{8}\sigma(\partial_i\sqrt{T})(\partial_i v_j+\partial_j v_i - \delta_{ij}\partial_l v_l)+\frac{\sqrt{\pi}}{8}\sigma\sqrt{T}\Delta v_j, \quad (3)$$

$$\dot{\nu}=-\partial_i(\nu v_i), \quad (4)$$

where T is the granular temperature and ν is the area fraction, σ is the diameter of a particle and ∂_i denotes $\partial/\partial r_i$, where $i=1,2$ denote the Cartesian components of the position vector $\mathbf{r}$. The summation convention for repeated indices is assumed. The coefficient of restitution, $\tilde{e}$, appears in $\epsilon=1-\tilde{e}^2$, and $\mathrm{Tr}\,\hat{D}_{ij}^2$ is the viscous heating function given by $\mathrm{Tr}\,\hat{D}_{ij}^2=\frac{1}{2}[(\partial_j v_i)(\partial_i v_j)+(\partial_j v_i)^2-(\partial_l v_l)^2]$. Equations (2)–(4) admit a basic solution with constant area fraction ν_0 (notice that the average area fraction, when referring to numerical results, is denoted by $\bar{\nu}$) constant temperature T_0 and a velocity field $\mathbf{v}=(\gamma y,0)$. The value of T_0 in the steady state is determined by the balance between the rate of viscous heating and collisional cooling

$$T_0=\frac{2l^2\gamma^2}{\pi\epsilon}. \quad (5)$$

where $l=\pi\sigma/8\nu_0$ is the mean free path in the homogeneous state. Similar (linearized) equations have been analyzed in Refs. 23–25. There the coordinates of the fields were transformed to frames of reference that move with the local mean flow; this procedure eliminates the coordinate-dependent convective terms in the original linearized equations, at the price of defining modes in terms of time dependent wave vectors. The resulting equations are not self-adjoint. Initial disturbances are found to grow for short times (the growth rates depending on the nature of the variables used in the analysis, a point discussed in Ref. 29) and then decay. It can be proven[25] that simple shear flow is asymptotically linearly stable, though there can be transient growth of infinitesimal disturbances. In contrast to the above studies, we consider the transient evolution of infinitesimal disturbances of the

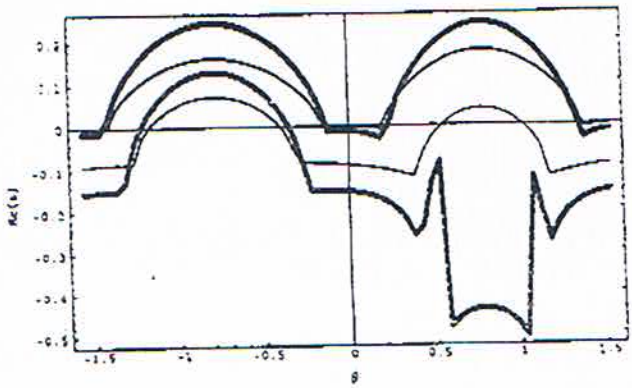

FIG. 15. The leading solution of the characteristic equation as a function of the wave number. The thick lines correspond $\epsilon=0.8$ and the thin lines to $\epsilon=0.2$. The gray lines correspond to an angle of 45° in wave number space and the black lines to an angle of 135°.

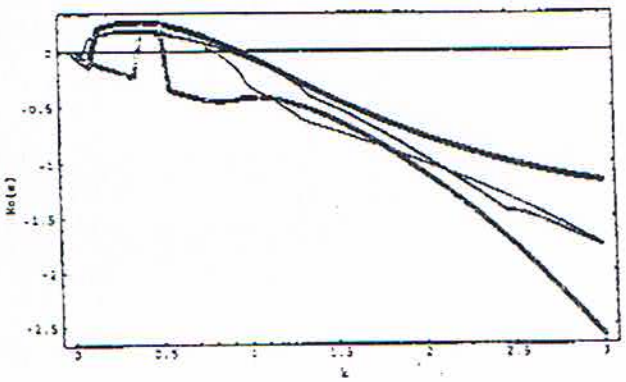

FIG. 16. The leading solution of the characteristic equation as a function of angle in the k space. The thick lines correspond to $\epsilon=0.8$ and the thin lines to $\epsilon=0.2$. The grey lines correspond to $k=0.75$ and the the black lines to $k=0.5$. The linear size of the system is normalized to 1.

basic state *for times which are short enough for the effect of convection to be negligible* (i.e., shorter than the inverse shear rate $\tau_c=1/\dot{\gamma}$), since clustering occurs on even shorter time scales.

In the following, it is convenient to nondimensionalize Eqs. (2)–(4) by measuring time in units of τ_c and length in units of $\sqrt{(2/\pi)}L_*$ and normalizing the area fraction ν and temperature T by their respective homogeneous values (in the time independent solution) ν_0 and T_0. Upon linearizing around the steady solution (in which the rescaled T and ν equal unity and the velocity field is $y\hat{x}$), one obtains

$$\delta\dot{T}=-\text{div}\ \delta\mathbf{v}-\sqrt{2\epsilon}\delta\nu-\sqrt{\frac{\epsilon}{2}}\,\delta T + \sqrt{2\epsilon}(\partial_1\delta v_2+\partial_2\delta v_1)+\sqrt{2\epsilon}\Delta\,\delta T, \tag{6}$$

$$\delta\dot{v}_j=-(\partial_j\delta\nu+\partial_j\delta T)+\sqrt{\frac{\epsilon}{8}}\,(\delta_{j1}\partial_2\delta T+\delta_{j2}\partial_1\delta T) + \sqrt{\frac{\epsilon}{2}}\,\Delta\,\delta v_j, \tag{7}$$

$$\delta\dot{\nu}=-\text{div}\ \delta\mathbf{v}, \tag{8}$$

where the notation is obvious. Assuming eigenmodes of the form $\exp(i\mathbf{k}\cdot\mathbf{r}+st)$ one obtains a fourth order characteristic equation in s (as a function of $\bar{\epsilon}$ and $\mathbf{k}$). The growth rates of the most unstable solution [largest Re(s)] are depicted as a function of the angle (of the wave vector) for two values of the wave number in Fig. 15 and as a function of the wave number for angles of 45° and 135°—in Fig. 16. Results are presented for two values of $\epsilon=1-\bar{\epsilon}t^2$. The leading instability points in the 45° direction in wave number space, as mentioned above. As mentioned, the maximal growth rate is disturbingly far smaller than the shear rate. One may conclude that linear stability analysis provides an indication of the nature of the unstable modes but it cannot explain their growth rates. Notice, however, that the development of the observed mode from the initial homogeneous state (cf. Fig. 14) occurs on a time scale which is larger than τ_c. Also notice that the stability equations analyzed in the above may not be accurate for the low value of $\bar{\epsilon}$ for which simulations are reported (much higher values of $\bar{\epsilon}$ require a much larger number of particles in order to observe the clustering dynamics). In any case, it is evident that nonlinearities take over at an early time.

B. Nonlinear mechanism and multistability

A large enough granular system, and therefore one having a large number of degrees of freedom, experiences statistical fluctuations of every macroscopic physical quantity except those that are strictly conserved. Consider a sheared hard-disk fluid at an initial temperature T_i. Such a system may have a shear fluctuation of the form $\delta\mathbf{v}=(0,v_0\sin kx)$, where k is consistent with periodic boundary conditions in a finite domain. Since equipartition is expected to hold during early times before the dynamics of the system becomes dominated by clustering, the typical amplitude v_0 of such a fluctuation can be estimated by computing the energy stored in the velocity field corresponding to this fluctuation and comparing the result to mT_i, which is the energy per degree of freedom (m is the mass of a particle). By equipartition, the energy E_s stored in a single shear mode $\delta\mathbf{v}=(0,v_0\sin kx)$ is $E_s=\rho v_0^2L^2$, where L is the linear dimension of the flow domain. Thus, $E_s\sim mT_i$ implies that $v_0\sim\sqrt{T_i/N}$, where N is the total number of particles in the system, and therefore the typical magnitude of $h=\partial\delta v_2/\partial x$ is $h\sim k\sqrt{T_i/N}$. Let the value of k^{-1} correspond to the expected dominant length scale (i.e., the intercluster separation; see below). If we assume that k^{-1} is long enough so that diffusion effects can be neglected with respect to viscous heating and inelastic dissipation (an assumption to be verified *a posteriori*) then we can approximate Eq. (2) by

$$\nu\dot{T}\simeq\frac{\sqrt{\pi}}{16}\,\sigma\sqrt{T}\ \text{Tr}\,\hat{D}_{ij}^2-\frac{8}{\sqrt{\pi}}\frac{\nu^2}{\sigma}\,\epsilon T^{3/2}. \tag{9}$$

Note that we are still considering the dynamics of the system at early times when the effect of convection can be neglected. Consider first the case when the initial temperature T_i is so large that h is large compared to $\dot{\gamma}$. This happens

The viscous heating function in this case can be approximated as follows:

$$\mathrm{Tr}\,\hat{D}_{ij}^2 \simeq \frac{1}{2}(\gamma+h)^2 \simeq \frac{1}{2}h^2\left(1+\frac{2\gamma}{h}\right)+O\left(\frac{\gamma^2}{h^2}\right), \quad h \gg \gamma. \tag{10}$$

Assuming that the density can be considered to be fixed in Eq. (9) and that the shear fluctuation is practically stationary with respect to the rate of decay of the temperature to its asymptotic value (assumptions again to be justified *a posteriori*), it can be shown that the solution to Eq. (9) is

$$T(t) = \frac{l^2h^2}{\pi\epsilon}A(t)\left(1+\frac{2\gamma}{h}\right)+O\left(\frac{\gamma^2}{h^2}\right), \tag{11}$$

where

$$A(t) = \left[\frac{1-\alpha\exp(-\sqrt{\epsilon}ht)}{1+\alpha\exp(-\sqrt{\epsilon}ht)}\right]^2 \tag{12}$$

and

$$\alpha \equiv [1-\sqrt{T_i/(l^2h^2/\pi\epsilon)}]/[1+\sqrt{T_i/(l^2h^2/\pi\epsilon)}]. \tag{13}$$

The condition that the diffusion term in Eq. (2) can be neglected relative to, say, the inelastic dissipation term is[16] $kl < \sqrt{\epsilon}$. The same condition ensures that diffusion is slow relative to the rate of saturation of $T(t)$ to its final value and that the shear fluctuation is quasistationary. When $\gamma/h \ll 1$, the temperature rapidly saturates to the value dictated by the (local) velocity field corresponding to the shear fluctuation and a corresponding temperature gradient is formed in the system. As a result, a pressure gradient is established as well. The local value of the pressure is given, to a good degree of approximation, by:

$$P = \rho_s \nu T \simeq \rho_s \nu \frac{l^2h^2}{\pi\epsilon}A(t).$$

Since $l=\pi\sigma/8\nu$, we have $P \sim \rho_s\sigma^2h^2/\epsilon\nu$ i.e., the pressure that is established is inversely proportional to the density. Thus the pressure in dense regions is low relative to the pressure in dilute regions rendering the clustering mechanism presented in Ref. 16 relevant here as well. The time scale for mass motion leading to clustering can be estimated from the part of Eq. (3) which contains the pressure induced forces alone: $\rho\dot{v} = -\nabla P$. Using Eq. (4), it follows that $\ddot{\rho} = \Delta P$ and the time scale, τ_m, for mass motion is easily seen to be

$$\tau_m \sim \frac{1}{k}\sqrt{\frac{\rho}{P}} \sim \frac{\sqrt{\epsilon}}{klh}. \tag{14}$$

The condition that τ_m be shorter than the convective time scale τ_c is therefore: $(\gamma/h)\sqrt{\epsilon} < kl$. All in all: $\sqrt{\epsilon}\gamma/h < kl < \sqrt{\epsilon}$. Since τ_m is shorter the larger the value of k (it takes less time for mass to move a distance k^{-1} the shorter the distance), the fastest and dominant clustering process will occur at the largest allowed value of k. Thus the clustering process occurs on the scale determined by $kl \sim \sqrt{\epsilon}$ [as in the unforced case (Ref. 16)]. Since mass accumulates at the minima of h (where the temperature is lowest), this scale corresponds to the typical separation between clusters in the flow.

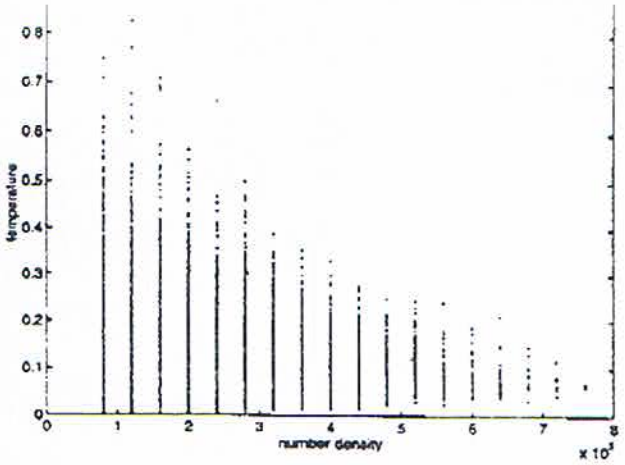

FIG. 17. The scatter plot of temperature vs number density in System II. The values of the temperature and number density are calculated by dividing the domain into 200×200 cells.

In the case $\gamma/h \gg 1$ (i.e., $T_i < T_0$) thermal equilibration (to the value T_0) occurs on a time scale of $O[(2\sqrt{2})/(\gamma\sqrt{\epsilon})]$ [following Eq. (9)] i.e., one that is larger than τ_c. The typical time scale for mass motion (in the beginning of the process) is $1/(k\sqrt{T_i})$ and the condition for mass to accumulate before thermal equilibration sets in is $1/(k\sqrt{T_i}) < 1/\gamma$, or, $kl > (\gamma l)/(\sqrt{T_i})$. The condition $kl < \sqrt{\epsilon}$ is still needed to ensure that diffusive effects do not dominate. These two conditions imply $T_i > T_0$, contrary to the assumption $T_i < T_0$. Thus the mechanism of clustering cannot operate in this case. Indeed, in this case numerical simulations reveal growing modes in both the 45° and 135° degrees directions in the density field during early times—yet no clustering. In contrast, when $\gamma/h \ll 1$, the nonlinear instability sets in much before these modes have a chance to significantly grow in amplitude. A state of "churn flow" is then observed (see below). In the case $\gamma/h \gg 1$, clustering is still possible but only at later times, when $T(t)$ increases to its asymptotic value. Here one obtains cluster interactions as described above (and the condition for clustering can be satisfied since the temperature is given by T_0). It is important to note that once the clusters have matured (i.e., stopped growing) the pressure in their interior is not different from the ambient pressure. Since the density in the mature clusters is relatively high, the temperature in their interior remains low. Figure 17 presents a scatter plot of temperature vs density in System II based on a division of the domain into a grid of 200×200 cells (the temperature and density in each cell are measured and pairs of values of the former and the latter are plotted in the figure). The large fluctuations observed are due to the small number of particles in each cell. The overall trend—the temperature being a decreasing function of number density—is evident.

To reprise, the two flow states shown in Figs. 18 and 19 are reached by the same system (asymptotically) after long times, correspond respectively to the case in which $T_i < T_0$

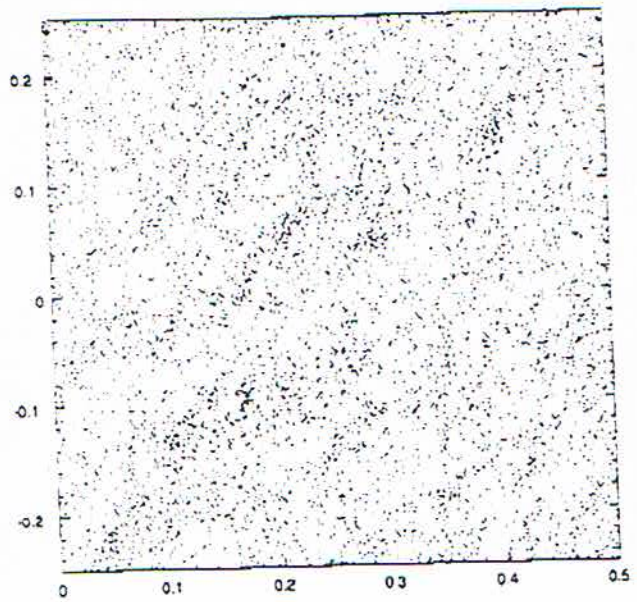

FIG. 18. The particle configuration of a quasihomogeneous shear flow at steady state. The portion of the flow domain shown here corresponds to a square region in the center of the system whose area is 1/4 the area of the system. The parameters characterizing the flow are: $\bar{\epsilon}=0.6$, $\bar{\nu}=0.05$, $N=20\,000$.

and that in which $T_i \gg T_0$. The numerical simulations reveal that the dynamical histories of these two systems are very different. In the former system, clusters appear uniformly and simultaneously throughout the system and are dispersed by convection and scattering on a time scale that is comparable to the time scale for the mass agglomeration that creates them. Since clusters are mass attractors and two clusters close together will coalesce, the fact that the agglomeration time scale is comparable to the dispersive one ensures that a stronger clustering effect does not occur and that the clusters remain relatively small in size. This is not the case for the churn flow depicted in Fig. 19, since the initial mass agglomeration time scale, being inversely proportional to the square root of the transient temperature, is so fast that convection by the mean shear has no time to act on the clusters that are formed. Nevertheless, convection in this case plays a role at later times by gradually sweeping the clusters together and causing them to coalesce into extended regions of high density. Thus, that the history dependence or hysteresis in shear flows arises because of the dependence of the time scale for mass agglomeration on the transient temperature. When this time scale is short, most of the mass of the system becomes rapidly entrapped in clusters, leaving a very dilute and voluminous ambient. The subsequent dynamics of the system becomes dominated by the dense clusters that are formed. When the time scale for mass agglomeration is comparable to those of the convection and diffusion, the latter processes continually rehomogenize the flow. Still another state (plug flow)[10] can be obtained with the same external parameters when the shear rate is built up in a time dependent fashion.

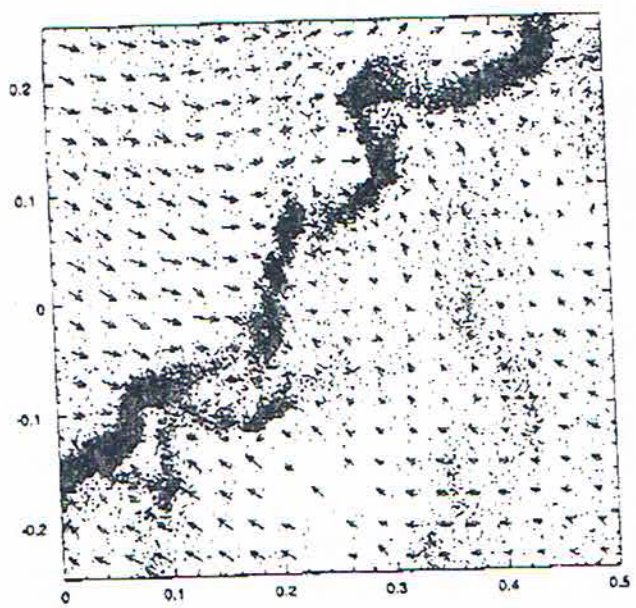

FIG. 19. The particle configuration of a churn shear flow at steady state on which a vector plot of the velocity field is superposed. The portion of the flow domain shown here corresponds to a square region in the center of the system whose area is 1/4 the area of the system. The parameters characterizing the flow are the same as those of the flow shown in Fig. 18.

V. CONCLUSION

We have shown that microstructures play a dominant role in the dynamics of sheared granular flows. They determine not only the properties of a given system but are also responsible for hysteretic effects. Clusters may interact as macroparticles and exhibit scattering, mutual annihilation and revival effects. On the basis of the results presented in this paper we conclude that no theory of granular systems is complete without a proper accounting of the microstructures.

ACKNOWLEDGMENTS

One of us (I.G.) wishes to gratefully acknowledge partial support from the National Science Foundation and the U.S.–Israel Binational Science Foundation.

[1]R. P. Behringer, "The dynamics of flowing sand," Nonlinear Sci. Today 3(3), 1 (1993).
[2]C. S. Campbell, "Rapid granular flows," Annu. Rev. Fluid Mech. 22, 57 (1990).
[3]C. S. Campbell and A. Gong, "The stress tensor in a two-dimensional granular shear flow," J. Fluid Mech. 164, 107 (1986).
[4]C. S. Campbell, "The stress tensor for simple shear flows of a granular material," J. Fluid Mech. 203, 449 (1989).
[5]S. McNamara and W. R. Young, "Inelastic collapse and clumping in a one-dimensional granular medium," Phys. Fluids A 4, 496 (1992).
[6]S. McNamara and W. R. Young, "Kinetics of a one dimensional granular medium in the quasielastic limit," Phys. Fluids A 5, 34 (1993).
[7]N. Sela and I. Goldhirsch, "Hydrodynamics of a one dimensional granular medium," Phys. Fluids 7, 507 (1995).
[8]O. Zik, D. Levine, S. G. Lipson, S. Shtrikman, and J. Stavans, "Rotationally induced segregation of granular materials," Phys. Rev. Lett. 73, 664 (1994).
[9]H. J. Herrmann, "Simulation of granular media," Physica A 191, 263 (1992).
[10]M-L. Tan, *Microstructures and Macrostructures in Granular Shear Flows*, Ph.D. thesis, Princeton University, 1995.
[11]R. H. Weiland, Y. P. Fessas, and B. V. Ramarao, "On instabilities arising

during sedimentation of two-component mixtures of solids." J. Fluid Mech. 142, 383 (1984).
[12]G. K. Batchelor and R. W. Janse van Rensburg, "Structure formation in bidisperse sedimentation," J. Fluid Mech. 166, 379 (1986).
[13]J. F. Brady and G. Bossis, "Stokesian dynamics," Annu. Rev. Fluid Mech. 20, 111 (1988).
[14]R. Jackson, "Hydrodynamic stability of fluid particle systems," edited by J. F. Davidson, R. Clift, and D. Harrison, *Fluidization* (Academic, New York, 1985).
[15]I. Goldhirsch and G. Zanetti, "Clustering instability in dissipative gases," Phys. Rev. Lett. 70, 1619 (1993).
[16]I. Goldhirsch, M-L. Tan, and G. Zanetti, "A molecular dynamical study of granular fluids I: The unforced granular gas in two dimensions," J. Sci. Comp. 8(1), 1 (1993).
[17]I. Goldhirsch and M-L. Tan, "The single-particle distribution function for rapid granular shear flows," Phys. Fluids 8, 1752 (1996).
[18]A. W. Lees and S. F. Edwards, "The computer study of transport processes under extreme conditions," J. Phys. C: Solid State Phys. 5, 1921 (1972).
[19]O. R. Walton and R. L. Braun, "Viscosity and temperature calculations for shearing assemblies of inelastic, frictional disks," J. Rheol. 30, 949 (1986).
[20]O. R. Walton and R. L. Braun, "Stress calculations for assemblies of inelastic spheres in uniform shear," Acta Mechanica 63, 73 (1986).
[21]M. A. Hopkins and M. Y. Louge, "Inelastic microstructure in rapid granular flows of smooth disks," Phys. Fluids A 3, 47 (1991).
[22]D. C. Rapaport, "The event scheduling problem in molecular dynamics simulation," J. Comp. Phys. 34, 184 (1980).
[23]P. J. Schmid and H. K. Kytömaa, "Transient and asymptotic stability of granular shear flow," J. Fluid Mech. 264, 255 (1994).
[24]S. B. Savage, "Instability of an unbounded uniform granular shear flow," J. Fluid Mech. 241, 109 (1992).
[25]M. Babic, "On the stability of rapid granular flows," J. Fluid Mech. 254, 127 (1993).
[26]J. T. Jenkins and M. W. Richman, "Grad's 13-moment system for a dense gas of inelastic spheres," Arch. Rat. Mech. Anal. 87, 355 (1985).
[27]C. K. K. Lun, S. B. Savage, D. J. Jeffrey, and N. Chepurniy, "Kinetic theories of granular flow: Inelastic particles in a couette flow and slightly inelastic particles in a general flow field," J. Fluid Mech. 140, 223 (1984).
[28]J. T. Jenkins and M. W. Richman, "Kinetic theory for plane flows of a dense gas of identical, rough, inelastic, circular disks," Phys. Fluids 28, 3485 (1985).
[29]S. McNamara, "Hydrodynamic modes of a uniform granular medium," Phys. Fluids A 5, 3056 (1993).